International Journal of Neural Systems, Vol. 0, No. 0 (2005) 1–22

A Neuronal Network Model of the Primate Visual System: Color Mechanisms in the Retina, LGN and V1

Pablo Martínez-Cañada, Christian Morillas and Francisco Pelayo*
Department of Computer Architecture and Technology, University of Granada, Granada, Spain
Centro de Investigación en Tecnologías de la Información y de las Comunicaciones (CITIC), University of Granada, Granada, Spain
{*pablomc,cmg,fpelayo*}*@ugr.es*

Color plays a key role in human vision but the neural machinery that underlies the transformation from stimulus to perception is not well understood. Here, we implemented a two-dimensional network model of the first stages in the primate parvocellular pathway (retina, lateral geniculate nucleus and layer 4Cβ in V1) consisting of conductance-based point neurons. Model parameters were tuned based on physiological and anatomical data from the primate foveal and parafoveal vision, the most relevant visual field areas for color vision. We exhaustively benchmarked the model against well-established chromatic and achromatic visual stimuli, showing spatial and temporal responses of the model to disk- and ring-shaped light flashes, spatially uniform squares and sine-wave gratings of varying spatial frequency. The spatiotemporal patterns of parvocellular cells and cortical cells are consistent with their classification into chromatically single-opponent and double-opponent groups, and non-opponent cells selective for luminance stimuli. The model was implemented in the widely used neural simulation tool NEST and released as open source software. The aim of our modeling is to provide a biologically realistic framework within which a broad range of neuronal interactions can be examined at several different levels, with a focus on understanding how color information is processed.

Keywords: Primate Visual System; Computational Model; Color Coding; Population Dynamics; Parvocellular Pathway; Red-Green Opponency; Retina; LGN; Primary Visual Cortex; V1.

1. Introduction

The perception of color is a fundamental property of primate vision.[1] Besides providing an aesthetic component to visual experiences, color facilitates object recognition, and has an important role in image segmentation and visual memory.[2,3] Since the early recordings of color-opponency in the first stages of the visual pathway,[4,5] color mechanisms have been studied physiologically,[5–11] psychophysically[12–14] and computationally.[15,16] However, many of these mechanisms are not well understood and much remains to be learned about the physiological basis of color perception. Therefore, understanding the neuronal basis of color coding is a necessity for a full description of the human visual processing.

The neural code for trichromatic color vision begins in the retina, when the visual stimulus is sampled by three cone photoreceptor types, sensitive to long (L cones), middle (M cones), or short (S cones) wavelengths. Cone signals are subsequently transformed into spectrally opponent responses through two different parallel processing streams in the retina, commonly known as red-green and blue-yellow pathways.[17,18] Each pathway is as-

*Corresponding author.

sociated with distinctive retinal architectures. The focus of this work is on the red-green pathway, in which signals from L and M cones are opposed.

Red-green opponency is a characteristic feature of the visual response of midget cells in the retina. The largest degree of color opponency has been observed in the central retina, fovea and parafovea, in which anatomical studies revealed that the receptive field center of midget cells is derived from a single L or M cone.[17,19] The visual field area of the fovea is thus the best candidate to study color mechanisms. Midget ganglion cells transmit red-green opponent signals to the parvocellular layers of the lateral geniculate nucleus (LGN) and parvocellular cells project, in turn, mainly to layer 4Cβ in the primary visual cortex (V1).[20–22] The parvocellular pathway can be considered the central pathway in color vision because about 80 % of retinogeniculate connections project to parvocellular layers[23] as well as 80 % of geniculocortical connections to striate cortex are from parvocellular LGN cells.[16]

To examine the neural mechanisms of color at the different stages of the visual path, we implemented a neuronal network model of the parvocellular pathway, from retina to V1 layer 4Cβ, based on physiological and anatomical data of the primate foveal and parafoveal vision. The model is based on a recently developed network model of the primate retina.[24] To make the model sufficiently representative, we chose those parameter values that best reflect the "mean" behavior of the whole population of neurons and discarded those features observed only in reduced numbers of neurons. Our design strategy has been to first set the morphological properties of the network, e.g., spatial extent of connections between different cell types, based strictly on experimental data from the literature. We then calibrated values of synaptic weights following some general connectivity rules to produce a model response that fits the physiological response.

With the exception of the remarkable modeling work by De Valois and De Valois,[16] there are few biological models of color processing specifically tuned to the primate visual system.[25–27] However, there is a greater number of models of the primate derived from the magnocellular pathway[28–32] and models in which the parvocellular pathway is included but the analysis of color mechanisms is neglected.[33] The numerous articles coauthored by R. Shapley[28–32] propose large-scale models, constructed also with conductance-based point neurons, for the study of different aspects of orientation selectivity in layer 4Cα. They are designed largely from data for the anatomy and physiology of the macaque. One of their major observations is that recurrent intracortical interactions play a major role in sharpening the orientation selectivity and filling in the gaps of orientations not represented by LGN.

The major limiting factor that continue to hinder the development of biophysical models of the primate visual system is the scarcity of physiological data from this species. Moreover, with regard to the modeling of the primate retina, there is a lack of standardized neuron models for neurons that communicate via graded potentials instead of spikes, as happens with most retinal neuron types (but not ganglion cells). Our model aims to provide solutions to these challenges and to serve as a realistic simulation framework within which several hypotheses of the neural coding of color vision can be explored.

At every stage of the model, a mechanistic description is given of the corresponding visual stage, including the retina (unlike other biophysical models of the mammalian thalamocortical system[34,35]). Neuronal layers of the network are built upon point neuron models, which have been widely used in large-scale models focused on neural interactions at the level of population coding because of the trade-off they can achieve between computational complexity and biological accuracy.[33,35,36] The model was validated against well-known visual stimuli commonly employed in electrophysiological experiments: disk- and ring-shaped light flashes, spatially uniform squares and sine-wave gratings of varying spatial frequency. It was also designed with the aim of being adaptable to different experimental setups and computational resources. Thus, one interesting property is that the population size can be scaled, while the model response remains unchanged. For the purpose of independent validation and further scientific exploration, the model was implemented using a well-established simulation tool, NEST 2.12.0,[37] and the code has been released as open source software.[38]

The rest of the article is organized as follows. In Section 2, we describe the overall architecture and connectivity of the network model and dynamics of the different neuron models. We then detail the specific implementation of each visual stage and

the methods used to simulate and analyze the data. The model was benchmarked against commonly used visual patterns (Section 3): light flashes of different shape and size, used first to calibrate the model response, and sine-wave gratings and spatially uniform squares. Finally, in Section 4, we discuss the nature of the model and its possible implications for understanding color vision.

2. Methods

2.1. *Overview of the network architecture*

The core of the network model comprises two-dimensional grids of neurons of the retina, LGN and layer 4Cβ in V1, as shown in the left diagram of Fig. 1. Each layer is scaled to span a patch of 2 deg $\times$ 2 deg of the foveal visual field and contains 40 $\times$ 40 neurons, except in the case of V1 layers for which there are 80 $\times$ 80 neurons. The cortical magnification factor of a foveal region in V1 ($<$ 2 deg) is estimated to be between 4 and 16 mm/deg.[39,40] Assuming the most conservative estimate of 4 mm/deg, a 2 deg $\times$ 2 deg patch in the fovea of our model V1 would correspond to 64 mm^2 of striate cortical surface. On the primate retina, one degree of visual angle in the fovea represents between 200 and 300 μm of retinal distance,[41] which implies that a 2 deg $\times$ 2 deg patch would have a surface area of 0.16 - 0.36 mm^2 in our model layers.

The model includes those visual stages that are involved in the key aspects of color processing in the parvocellular pathway. Here, we provide a summary of the main properties of the network circuitry. Please refer to the following sections for a detailed explanation of each stage.

The vertical pathway of the earliest stage, the retina, is well-established, consisting of L and M cones, midget bipolar cells and midget ganglion cells (Fig. 1, right panel). As observed experimentally in the fovea, there is a one-to-one relationship between cones to midget bipolar cells, which receive input from a single cone type, L or M type, and between midget bipolar cells to midget ganglion cells.[17] Horizontal connections in the parvocellular pathway are formed by H1 horizontal cells and amacrine cells. H1 horizontal cells receive indiscriminate input from an extended region of L and M cones and do not transmit an S-cone signal.[17] H1 horizontal cells also synapse onto bipolar cells, providing an inhibitory signal that is the basis of the inhibitory surround of the bipolar-cell receptive field. Among all types of amacrine cells, the model includes only the AII amacrine cell since it is the most studied amacrine cell and the most numerous type in the mammalian retina.[42] Under cone-driven conditions, ON-center bipolar cells excite AII amacrine cells through gap junctions and, in turn, AII amacrine cells release inhibitory neurotransmitters onto OFF bipolar cells and OFF ganglion cells.[43,44]

Midget bipolar cells react to visual stimuli with two different responses, ON-center and OFF-center responses,[45,46] described in the model by different activation functions at the cone bipolar-cell synapse ($g(V_c)$ in the insets of Fig. 1). ON-center bipolar cells depolarize with light increments while OFF-center bipolar cells depolarize when the intensity of the stimulus is reduced. Combining all alternatives, cone-type specificity of bipolar cells and the different activation functions of their synaptic channel, there are 4 possible chromatic signals, L-ON, L-OFF, M-ON and M-OFF, which are originated in midget bipolar cells and integrally transmitted to midget ganglion cells.

The next stage of the model is the parvocellular laminae of the LGN (layers 3-6), which contain relay cells and interneurons. In primate, there are about as many relay cells as ganglion cells and there is nearly a one-to-one anatomical mapping from retina to relay cells.[47] As a consequence, relay cells inherit similar receptive-field properties of ganglion cells and show the 4 types of chromatic responses: L-ON, L-OFF, M-ON and M-OFF.

A number of studies have revealed that almost all neurons in laminae 5 and 6 are ON-center cells, whereas layers 3 and 4 contain mostly OFF-center neurons.[48–50] Thus, ON and OFF cells in the model, both relay cells and interneurons, remain functionally separated at the LGN. Interneurons have electrophysiological properties similar to the relay cells in their laminae when using achromatic stimuli.[48] However, interneurons' dendrites are 2 or 3 times larger than relay cells' dendrites[48,51] so we assumed that interneurons can receive input from an extended region of both L- and M-type ganglion cells. Therefore, in the model circuit there are two types of interneurons, ON interneurons, located in the same laminae of L-ON and M-ON relay cells, and OFF interneu-

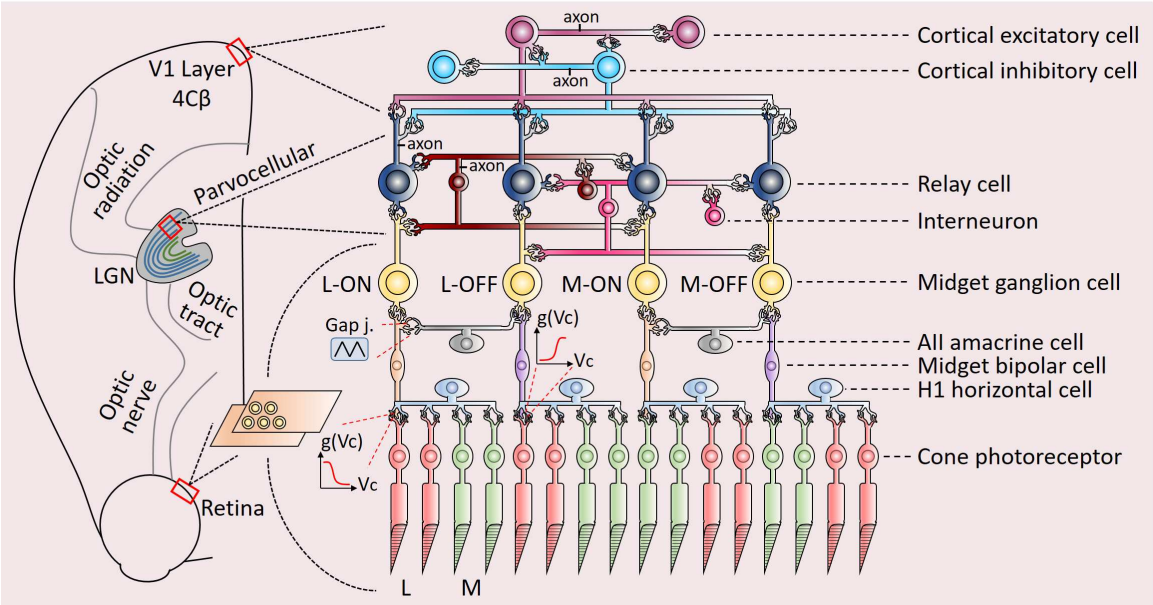

Figure 1. Schematic of the circuit model. The different visual stages of the model are indicated by red squares in the left diagram: retina, parvocellular laminae of the LGN and layer 4Cβ in V1. Each stage consists of two-dimensional grids of neurons, as illustrated for the retina stage. On the right, we depict the different cell types and their connectivity patterns.

rons, in the laminae of L-OFF and M-OFF relay cells. Interneurons synapse on relay cells, incorporating typically both axonal and triadic inhibition.[47] In macaque monkeys, though, triads appear to be common in the magnocellular layers and much rarer in the parvocellular layers.[52] We only modeled axonal inhibition.

Cortical neurons in layer 4Cβ of V1 are implemented as coupled populations of excitatory and inhibitory cells (which is in accordance with other modeling works[28,32]). Although model cortical neurons do not strictly match a specific cell type, parameters of excitatory cells were mainly extracted from measurements of spiny stellate cells because parvo inputs to the layer 4Cβ synapse principally on spiny stellate cells.[22] Evidence from anatomical data[53] and other modeling studies[28] suggests that three-quarters of cortical cells are excitatory cells and the rest are inhibitory cells. To meet the constraints of spatial uniformity in the two-dimensional distribution of cells in the grid, we used a slightly different proportion between excitatory and inhibitory cells, which is 80 % of excitatory cells and 20 % of inhibitory cells. As shown in Fig. 1, model cortical cells are synaptically coupled so that excitatory cells synapse both onto themselves and inhibitory cells and, similarly, inhibitory cells connect with both themselves and excitatory cells.

2.2. *Organization of receptive fields*

Models of the visual system often employ descriptive filters to reproduce the spatial properties of neurons' receptive fields.[54,55] In accordance with our mechanistic approach of modeling, we constructed receptive fields by shaping the spatial structure of synaptic connections. We used the masks included in the NEST Topology module[56] to define the area of nodes in the target layer to be connected by the source node. The probability of connection to target cells is constant within the area defined by the mask, in disagreement with other models in which this probability is dependent on distance.[28] Until recently, there had been little clear-cut evidence on whether probability of connection among adjacent neurons depends systematically on the distance between neurons.[57] Moreover, the spatial extent of a great number of connections in our model is minimal and applying a probability function to the connection would result in several neurons remaining isolated.

Receptive fields of midget bipolar cells already show the classical center-surround antagonistic structure of the retina.[17,58] In the model, cones

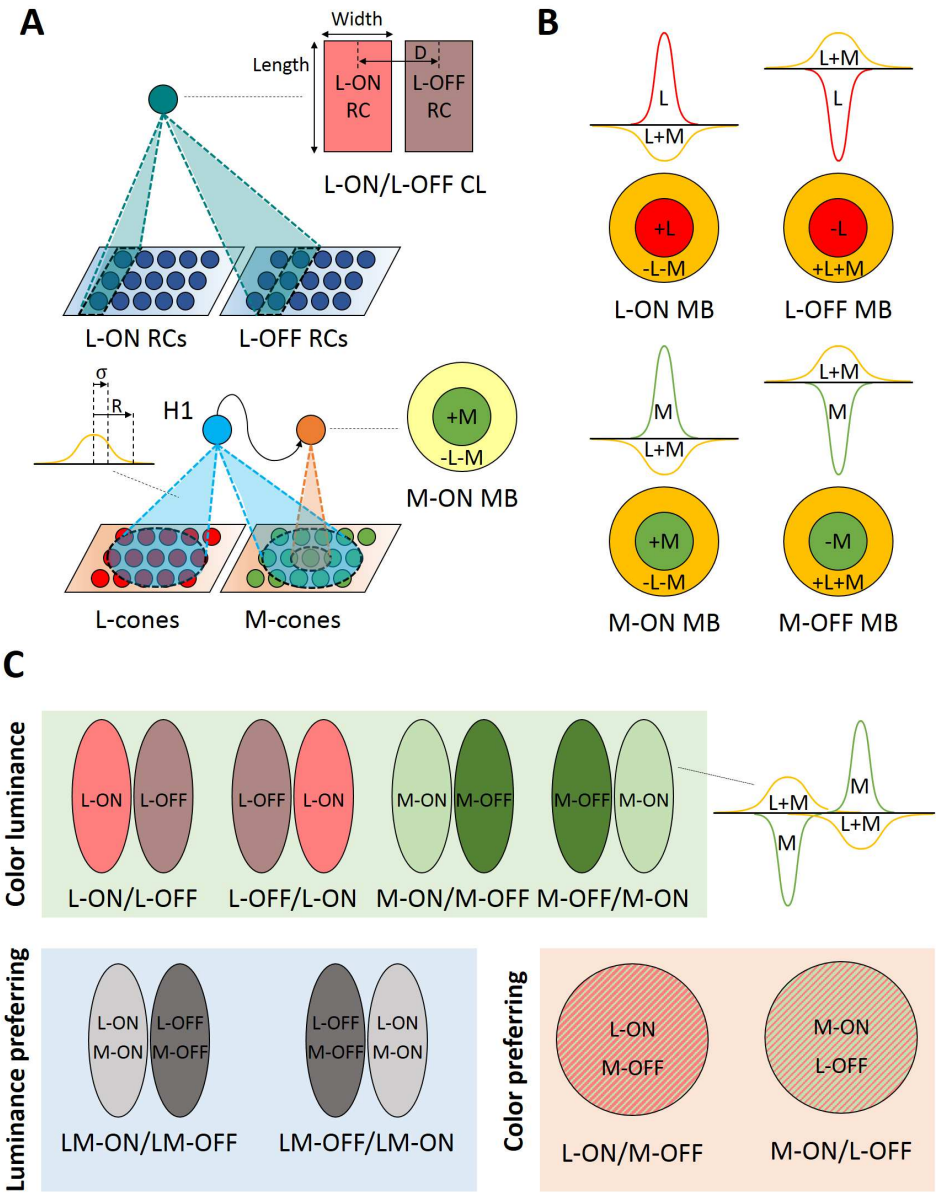

Figure 2. Formation of receptive fields of model neurons. A: Mask types used at the retina (bottom) and V1 (top) and description of parameters used to define circular masks (radius R and standard deviation σ) and rectangular masks (width, length and distance D). B: Hypothetical spatial sensitivity profiles and two-dimensional receptive fields of midget bipolar cells. L- and M-cone inputs to the neuron receptive field are indicated by '+' (excitatory) and '-' (inhibitory). C: Receptive fields of the different subpopulations of cortical cells and example spatial sensitivity profile of a double-opponent cell. Labels of each subregion represent the inputs from the different types of relay cells. H1 corresponds to H1 horizontal cell, MB is midget bipolar cell, RC is relay cell and CL is color-luminance.

are connected through circular masks of different sizes to horizontal cells and midget bipolar cells as shown in Fig. 2 A. The circularly symmetric center-surround mechanism at the bipolar-cell stage is created by combination of signals from horizontal cells and cones that are opposite in sign. This center-surround receptive field is inherited by midget ganglion cells and LGN relay cells because of the one-

to-one mapping between them. Weights of synaptic connections are generated according to a Gaussian distribution, resulting in the spatial sensitivity profiles shown in Fig. 2 B.

Formation of receptive fields of cortical cells may have a cortical origin, rather than an origin derived from the LGN input. However, we opted for a simplified receptive field organization based solely on LGN inputs. The feedforward input of cortical-cell receptive fields is built upon rectangular masks.[35] This type of mask facilitated the fitting of model parameters to the type of measurements used to estimate the receptive-field size of cortical cells.[40,59] Cortical cells that are selective for orientation of the stimulus, such as the vertically-selective neuron shown in Fig. 2 A, receive input from two adjacent rectangular regions of LGN relay cells. The overlap of circular receptive fields of LGN cells located within these rectangular regions result in the characteristic oval shape of each subregion in the cortical receptive field.

We divided the population of cortical cells into three groups in accordance with the studies of Johnson et al.:[7,10,60] luminance-preferring, color-luminance and color-preferring cells. Luminance-preferring cells show a minimal response to equiluminant gratings, but respond well to luminance patterns, color-luminance cells are spatially tuned for equiluminant and also for luminance patterns and color-preferring cells give large responses to equiluminant gratings and little response to luminance gratings. In the model, luminance-preferring cells are 60 % of the total amount of cortical cells, color-luminance cells are 30 % and color-preferring cells are 10 %, in agreement with experimental data of V1 cells.[20] Most luminance-preferring and color-luminance cells have oriented receptive fields with odd-symmetry: receptive fields formed by two adjacent elongated subregions, ON and OFF, of similar weights.[20,60] Color-preferring cells are not orientation selective and have subregions that are approximately circular in shape and concentric.[7]

Following these guidelines, together with other complementary physiological measures (addressed below), we come up with the minimal set of receptive fields given in Fig. 2 C. Receptive fields of color-luminance cells have subregions that are fed only by a single type of relay cell. For example, the L-ON/L-OFF receptive field has a left subregion that receives input from L-ON relay cells and a right subregion that is driven by L-OFF relay cells. Luminance-preferring receptive-fields have subregions that receive input from two types of relay cells but always of the same sign. In the LM-ON/LM-OFF receptive field, L-ON and M-ON relay cells synapse onto the left subregion and L-OFF and M-OFF relay cells onto the right subregion. There is only a single subregion for color-preferring cells, which receive input from both L-ON and M-OFF relay cells (L-ON/M-OFF receptive field) or from both M-ON and L-OFF relay cells (M-ON/L-OFF). Unlike LGN cells, receptive fields of color-preferring cells would be designated as Type II[20] because the spatial spread of center and surround are roughly identical.

2.3. *Neuron models*

All neurons in the network are implemented as single-compartment models. The basic equation describing the dynamics of the neurons' membrane potential, $V_m(t)$, for all types of neurons can be summarized as:[33,54,61,62]

$$\frac{dV_m(t)}{dt} = -g_L \frac{V_m(t) - E_L}{C_m} - \frac{I_{in}(t)}{C_m} + \frac{I_e}{C_m} \quad (1)$$

where g_L is the leak conductance, E_L the leak reversal potential, C_m the capacity of the membrane and I_e an (optional) constant external input current. Spiking cells (e.g., ganglion cells) also include integrate-and-fire dynamics based on a threshold potential, V_{th}, a reset voltage, V_{reset}, and a refractory period, t_{ref}. Ganglion cells also receive a Gaussian white noise current of zero-mean and standard deviation of 1 pA to prevent them from spike synchronization.

$I_{in}(t)$ represents either incoming synaptic currents or gap junction currents. For all cells except amacrine cells, $I_{in}(t)$ is the sum of excitatory and inhibitory synaptic currents:

$$\begin{aligned} I_{in}(t) = &\sum_{i=1}^{N} w_i g_i(t)(V_m(t) - E_{ex}) + \\ &+ \sum_{j=1}^{M} w_j g_j(t)(V_m(t) - E_{in}) \end{aligned} \quad (2)$$

w_i, w_j are synaptic weights and E_{ex}, E_{in} are the reversal potentials for the N excitatory synapses and the M inhibitory synapses respectively. In the case

of retinal cells, $g_i(t)$ and $g_j(t)$ are the synaptic activation functions of the neuron. Synaptic activation functions are modeled as a direct function of some presynaptic activity measure. In the simplest case, synaptic interactions are described by an instantaneous sigmoid function:[63,64]

$$g(t) = \frac{1}{1 + e^{-(V_{pre_i}(t) - \theta_{syn})/k_{syn}}} \quad (3)$$

where $V_{pre_i}(t)$ is the membrane potential of the neuron i and θ_{syn} and k_{syn} are parameters used to customize the sigmoid function. In the case of LGN cells and cortical cells, incoming spike events induce a post-synaptic change of conductance modeled by an alpha function:

$$g(t) = (t - t_{j,k})\frac{e}{\tau_{syn}} e^{-(t-t_{j,k})/\tau_{syn}}, \; for\; t > t_{j,k} \quad (4)$$

where $t_{j,k}$ is the time of the k^{th} spike arriving from neuron j and τ_{syn} is the time constant. For amacrine cells, $I_{in}(t)$ is the sum of gap junction currents through electrical synapses with a constant gap junction conductance (g_{gap}):

$$I_{in}(t) = \sum_{i=1}^{N} g_{gap}(V_m(t) - V_{pre_i}(t)) \quad (5)$$

Passive electrical properties are different for each cell type through the parvocellular pathway. In the retina, beyond the general classification of retinal cells into photoreceptors, horizontal, bipolar, amacrine and ganglion cells, each class is divided in turn into dozens of morphological distinct cell types.[42] Fitting the specific properties of every cell type is not within the scope of this study. Instead we specified some neuron parameters for all cells using commonly accepted values: $C_m = 100\ pF$, $g_L = 10\ nS$; and $V_{th} = -55\ mV$, $V_{reset} = E_L$ and $t_{ref} = 2\ ms$ for spiking cells. The leak reversal potential, E_L, of spiking neurons is set to -60 mV, consistent with the mean resting potential from in vivo intracellular recordings measured in others species.[65] E_L was adjusted in horizontal cells and bipolar cells to force a resting potential in the dark of about -45 mV (Table 1), as observed experimentally,[63,66] and in amacrine cells for a resting potential of about -65 mV. Values of the synaptic activation functions, θ_{syn} and k_{syn}, were set to force a synaptic threshold below resting potential,[63] in particular for bipolar cells.

Table 1. Summary of parameter values of neuron models. Parameters of activation functions of retinal cells, θ_{syn} and k_{syn}, correspond to the postsynaptic conductance. E_L, E_{ex}, E_{in} and θ_{syn} are expressed in mV, k_{syn} is unitless. H1 is H1 horizontal cell, MB is midget bipolar cell, AII is AII amacrine cell, MG is midget ganglion cell, RC is LGN relay cell, IN is LGN interneuron, CEX is cortical excitatory cell and CIN is cortical inhibitory cell.

	E_L	E_{ex}	E_{in}	θ_{syn}	k_{syn}
H1	-60	0	-	-50	4
ON MB	-60	0	-70	-37	2
OFF MB	-50	0	-70	-37	2
AII	-55	-	-	-55	4
MG	-60	0	-70	-	-
RC	-60	0	-80	-	-
IN	-60	0	-80	-	-
CEX	-60	0	-70	-	-
CIN	-60	0	-70	-	-

Reversal potentials of thalamic cells (RC and IN in Table 1) are more negative because of nucleus specific differences in the chloride reversal potential.[67] Time constants of alpha functions were selected to approximate $AMPA$ and $GABA_A$ functions used in other models of the thalamus:[35,68] $\tau_{syn,ex} = 1\ ms$ (excitatory) and $\tau_{syn,in} = 3\ ms$ (inhibitory).

2.4. *Retina*

Response of cones was implemented according to Van Hateren's model of primate cones[69] with linear cone-horizontal cell feedback. We opted for the linear cone-horizontal cell feedback instead of the nonlinear synaptic gain because a linear feedback is sufficient to capture the key properties of light adaptation, whereas the nonlinear gain simply adds a slight improvement of the fits to specific measurements. We chose the same generic parameter values given in Table 1 of the corresponding publication,[69] with the exception of parameter g_s, which was 0.5 instead of 8.81 to increase the overshoot of the response with a stimulus onset, allowing us to improve the fits to the wider repertoire of stimuli used in this work. The membrane potential of cones in our model corresponds to V_s in Fig. 5 A of Van Hateren's model.[69]

Photoreceptors release only one type of neurotransmitter, glutamate. However, bipolar cells react

Table 2. Parameter values of synaptic connections in the retina and LGN. H1 is H1 horizontal cell, MB is midget bipolar cell, AII is AII amacrine cell, MG is midget ganglion cell, RC is relay cell and IN is interneuron.

Source Layer	Target Layer	R(deg)	σ(deg)	W(nS)	τ(ms)
L-Cone	L-ON MB	0.09	0.03	5	1
L-Cone	L-OFF MB	0.09	0.03	6	1
L-Cone	H1	0.3	0.1	2	1
M-Cone	H1	0.3	0.1	2	1
H1	L-ON MB	0.3	0.1	3.5	5
H1	L-OFF MB	0.3	0.1	-6	5
AII	L-OFF MB	0.09	0.03	-1	1
AII	L-OFF MG	0.09	0.03	-1	1
L-ON MB	L-ON MG	0.09	0.03	30	1
L-OFF MB	L-ON MG	0.09	0.03	30	1
L-ON MG	L-ON RC	0.09	0.03	4	1
L-OFF MG	L-OFF RC	0.09	0.03	4	1
L-ON MG	ON IN	0.18	0.06	2	1
M-ON MG	ON IN	0.18	0.06	2	1
ON IN	L-ON RC	0.18	0.06	-2	2
ON IN	M-ON RC	0.18	0.06	-2	2
ON IN	ON IN	0.18	0.06	-2	2

to this stimulus with two different responses, ON-center and OFF-center responses.[45,46] While OFF bipolar cells have ionotropic receptors that maintain light-activated hyperpolarizations of photoreceptors, ON bipolar cells have instead metabotropic receptors that produce a sign reversal at the photoreceptor-ON bipolar cell synapse. Ionotropic glutamate receptors are positively coupled to the synaptic cation channel of OFF bipolar cells, which is opened with an increase of glutamate. On the contrary, ON bipolar cells are negatively coupled to the synaptic cation channel and glutamate acts essentially as an inhibitory transmitter, closing the cation channel.

To simulate the activation function of this cation channel based on the cone membrane potential ($V_{cone}(t)$), we used a sigmoid function whose exponent is negative for OFF bipolar cells (standard sigmoid) and positive for ON bipolar cells (inverted sigmoid):

$$g_{OFF}(t) = \frac{1}{1 + e^{-(V_{cone}(t) - \theta_{syn})/k_{syn}}} \tag{6}$$

$$g_{ON}(t) = \frac{1}{1 + e^{(V_{cone}(t) - \theta_{syn})/k_{syn}}} \tag{7}$$

For the synapse horizontal cell-bipolar cell, although both bipolar cell types express the same ionotropic GABA receptors, GABA release from horizontal cells can evoke opposite responses. One evidence suggests that GABA evokes opposite responses if chloride equilibrium potentials of the synaptic chloride channel in the two bipolar cell types are on opposite sides of the bipolar cell's resting potential.[70] In our model, ON bipolar cells receive excitatory synapses from horizontal cells, which have a positive reversal potential taking as a reference the bipolar cell's resting potential, and OFF bipolar cells receive inhibitory synapses, which have a negative reversal potential.

The summary of parameter values used for synaptic connections is shown in Table 2. Every cell in the source layer connects to all nodes in the target layer within a circular mask of radius R and with a delay τ. Weights of synaptic connections are generated according to a Gaussian distribution of standard deviation σ. For a single neuron, the sum of the weights of all incoming synapses is equal to the total weight W. W represents the peak value of fluctuations of the input conductance and is expressed in nS.

For connections of cells in the vertical pathway (bipolar cells and ganglion cells), we chose the value of σ (0.03 degrees) to match the size of the receptive-field center of parvocellular cells in the fovea.[71] The

parvocellular receptive-field surround is created at the horizontal-cell stage, where synaptic connections have a σ of 0.1 degrees. To reproduce the delayed response of the surround, which is estimated, on average, between 5 and 15 ms,[72] a delay of 5 ms was given to the connection from horizontal cells to bipolar cells. For ganglion cells, we chose larger presynaptic weights (30 nS) that keep the cell constantly depolarized, resulting in a spontaneous firing rate of 50 s^{-1} in response to a full-field stimulus of about 20 cd/m^2.[73]

2.5. *LGN*

In the cat, the receptive-field center of relay cells is driven by excitation of ganglion cells of the same sign (ON or OFF) and the surround apparently emerges through inhibition of interneurons that receive input from ganglion cells of the opposite sign.[47,74,75] Although there are some recordings of interneurons in the parvocellular laminae having center responses that are of the opposite sign of the relay cells around them,[48] evidence suggests that same-sign inhibition of relay cells is rather the general trend in the primate: first, ON and OFF cells, both relay cells and interneurons, remain functionally separated at the level of the LGN;[48–50] second, axons of interneurons often ramify locally within the boundaries of the thalamic nucleus of origin.[76] There are other models of the LGN that also implement same-sign inhibition from thalamic interneurons.[68,77]

Local interneurons are not the only elements involved in the role of inhibition in the thalamus: the GABAergic neurons of the reticular nucleus also project to the dorsal thalamic nuclei in all mammalian species. However, the neural density in the reticular thalamic nucleus is relatively low enough in the primate thalamus (3-5 cells per 62500 μm^2)[76,78] to consider the reticular nucleus as a potential candidate to be included in our model. Moreover, in a study of different mammalian species,[76] a progressive decrease is seen in the cellular density of neurons in the reticular nucleus from the bat to humans, that seemed to parallel the numerical increase of local interneurons. On this basis, it has been hypothesized that, with the increase in the number of local interneurons in the dorsal thalamus, the role of the reticular nucleus becomes more focused on the regulation of the sleep-waking cycle, acting as an internal thalamic pacemaker, rather than on direct inhibition of relay cells.

Parameters of synaptic connections of LGN cells (Table 2) were configured based on the observation that relay-cell receptive fields fairly replicate ganglion-cell receptive fields. Thus, synaptic connections between ganglion cells and relay cells maintain the same size of the receptive-field center of parvocellular cells (σ = 0.03 degrees). Synaptic weights of these connections were set to ensure that LGN transmits only a fraction of the retinal inputs it receives, typically 50 %.[77,79] Interneurons' dendrites are 2 times larger (σ = 0.06 degrees) than relay cell's dendrites based on anatomical data.[48,51]

2.6. *V1 layer 4Cβ*

Receptive fields of color-luminance and luminance-preferring cells are created by using two adjacent rectangular masks of the width and length specified in Table 3 and separated by a distance D. Synaptic weights of individual connections to the target cortical cell are all the same, and the sum of all the weights for a single neuron is equal to the total weight W.

To come up with parameter values shown in Table 3, we were guided by the following experimental constraints. The postsynaptic spiny stellate dendritic arbor in 4Cβ is 200 μm in diameter, matching the diameter of individual parvocellular thalamic axon arbors.[80,81] The total diameter of the field of terminations of parvocellular axons overlapping at least half the dendritic field of single spiny stellate neurons is therefore about 400 μm. Assuming a cortical magnification factor of 4 mm/deg, 400 μm would correspond to 0.1 degree of visual angle. Therefore we restricted the width and length of the mask and the separation distance D to an approximate value of 0.1 degrees.

The separation between subregions, D, was set to 0.1 degrees in agreement with physiological measures in the fovea (estimated on average between 0.1 and 0.2 degrees[82]). The distribution of receptive-field length/width ratios is seen to be nearly invariant with eccentricity in foveal striate cortex and the average value to be about 2.[40] Accordingly, we set the width of the rectangular mask to 0.052 degrees.

Parameters of intracortical connections are shown in Table 4. The different subpopulations of cortical cells are all-to-all coupled (e.g., L-ON/L-OFF vertically-oriented color-luminance cells are

Table 3. Parameter values of thalamocortical connections. RC is relay cell, CL is color-luminance cell, LP is luminance-preferring cell and CP is color-preferring cell. Each subpopulation of cortical cells is also divided into excitatory cells (Ex.) and inhibitory cells (In.).

Source Layer	Target Layer	Width (deg)	Length (deg)	D (deg)	W(nS)	τ(ms)
RC	Ex. CL	0.052	0.12	0.1	2.5	3
RC	Ex. LP	0.052	0.12	0.1	1.25	3
RC	Ex. CP	0.12	0.12	-	2.5	3
RC	In. CL	0.052	0.12	0.1	3	3
RC	In. LP	0.052	0.12	0.1	1.5	3
RC	In. CP	0.12	0.12	-	3	3

Table 4. Parameter values of intracortical connections. W corresponds to the sum of the weights for all individual connections that come from a single subpopulation (e.g., L-ON/L-OFF vertically-oriented color-luminance cells). The same value of W is used for incoming connections from all the different subpopulations of cortical cells.

Source Layer	Target Layer	R(deg)	σ(deg)	W(nS)	τ(ms)
Ex. cells	Ex. cells	0.15	0.05	0.5	2
Ex. cells	In. cells	0.15	0.05	0.5	2
In. cells	Ex. cells	0.075	0.025	-3	2
In. cells	In. cells	0.075	0.025	-3	2

connected with L-ON/L-OFF horizontally-oriented color-luminance cells, with L-OFF/L-ON vertically-oriented color-luminance cells and so on).

Parametrization of connections from excitatory cells is based on the experimental observation that axonal arborizations originating from spiny stellate cells are confined to within 2 dendritic arbor radii of the cell body (about 200 μm, 0.05 degrees).[83,84] Inhibitory cells in the model do not correspond to a specific type of inhibitory cell in V1. However, most interneurons have dendritic field and axon arbor extents of 300 μm or less in diameter.[80] Moreover, inhibitory interneurons do not generally form long range projections with their axon.[80] The axonal field of a type of GABA cell (clutch cell) in layer 4C was seen to be 100 - 150 μm in diameter.[85] It also seems clear that there are no long horizontal inhibitory connections in layer 4Cβ since wide-arbor basket neurons are found at all depths in V1 but not in layer 4Cβ.[80] Based on all these findings, inhibitory connections were assigned a value of 0.025 degrees (100 μm).

Cortico-cortical inhibition plays an important role in producing orientation tuning of cortical cells.[86] Experimental measures in the visual cortex have shown that excitatory conductances are generally lower in magnitude than inhibitory conductances.[87] Parameter values of synaptic weights (W) in Table 4 reflect the stronger coupling of inhibitory neurons to all other cortical neurons in rough agreement with other modeling studies of layer 4C in V1.[28,32]

2.7. *Visual stimuli and analysis of results*

The light intensities of the visual stimuli used in this study are expressed in units of trolands (td). This is a measure of retinal illuminance, defined as the area, in mm^2, of the pupil of the eye multiplied by the scene luminance, expressed in $candela/m^2$ (cd/m^2). Here, we use the approximation of 1 $cd/m^2 \approx 10$ td. The three main visual stimuli explored in the present work were: (i) light flashes of different shapes, (ii) spatially uniform red and black squares and (iii) sine-wave gratings of varying spatial frequency.

The contrast of achromatic stimuli (i.e., stimulus intensity/background intensity) was set to 0.8. Each trial was simulated for 1000 ms with a simulation resolution of 1 ms, and the experiment repeated for 400 trials. Membrane potentials and raw post-stimulus time histograms (PSTHs) were collected for all cells in the model. The PSTHs were averaged over

400 trials and used to obtain the estimated firing rates.

The dynamics of parvocellular receptive fields were explored with flashing spots and annuli concentric with the center of the two-dimensional grid. Each trial of the stimulus consisted of a 500 ms period of full-field equiluminant background followed by a 250 ms period in which the circular spot or the annulus intensity was superimposed on the background. There was another 250 ms period in which the stimulus returned to the background level. The full-field background was produced by a spatially uniform light intensity of 250 td per cone type (L- and M-cone), giving an estimated value of 500 td (50 cd/m^2) of mean luminance. 50 cd/m^2 is a typical value of mean luminance used in electrophysiological experiments.

We used spots of two sizes: a small spot (0.09-degree radius) to study center mechanisms of the receptive field and a full-field spot (0.5-degree radius) to elicit the center-surround antagonistic response. The full-field spot could be a white or a black spot based on whether the spot light intensity was added or subtracted from the equiluminant background respectively. The annulus stimulus was used to study surround mechanisms and its inner radius was 0.09 degrees and the outer radius 0.5 degrees. We show the trial-averaged traces of individual neurons and also the time-averaged topographic representation of responses of cells in the network grids. Each topographic map includes the activity of every cell in the corresponding two-dimensional grid, averaged across different time intervals.

For the second set of the experiments, red and black squares (1 deg × 1 deg) were presented on a full-field equiluminant background (50 cd/m^2). The red square is described mathematically as:

$$\begin{aligned} L_{input} &= I_{bkg}/2 + I_{stim}/2 \\ M_{input} &= I_{bkg}/2 - I_{stim}/2 \end{aligned} \tag{8}$$

where L_{input} and M_{input} are the light intensities received by L- and M-cones located within the square, I_{bkg} is the background intensity and I_{stim} the stimulus intensity. Therefore, the red square is equal in luminance to the background: $L_{input} + M_{input} = I_{bkg}$.

The cone contrast is computed from the amount of light intensities received by cones in the square (E_{square}) relative to light intensities received in the background (E_{bkg}) and expressed as:[88]

$$Cone_c = (E_{square} - E_{bkg})/E_{bkg} \tag{9}$$

The L-M cone contrast is computed as the difference between the cone contrast of L- and M-cones:

$$\begin{aligned} &(I_{bkg}/2 + I_{stim}/2 - I_{bkg}/2)/(I_{bkg}/2) - \\ &-(I_{bkg}/2 - I_{stim}/2 - I_{bkg}/2)/(I_{bkg}/2) = \\ &= I_{stim}/(I_{bkg}/2) = 2(I_{stim}/I_{bkg}) \end{aligned} \tag{10}$$

The black square is defined as:

$$\begin{aligned} L_{input} &= I_{bkg}/2 - I_{stim} \\ M_{input} &= I_{bkg}/2 - I_{stim} \end{aligned} \tag{11}$$

The luminance contrast of the black square ($(I_{bkg} - 2I_{stim} - I_{bkg})/I_{bkg} = -2(I_{stim}/I_{bkg})$) is similar to the L-M cone contrast of the red square but of opposite sign. For the square stimuli, we show the time-averaged topographic representations of selected cortical subpopulations.

The third stimulus consisted of full-field sinusoidal gratings with vertical orientation: luminance grating, red-green equiluminant grating and L- or M-cone-isolating gratings. All gratings have the same mean luminance and contrast. The red-green equiluminant gratings were produced by modulating the red and green intensities of cones in antiphase with equal amplitudes, but opposite sign. Stimuli for the two cone-isolating directions (L- and M-cone) were produced by adjusting the modulation of one cone to the sine wave and the other cone to the constant background level. To generate spatial frequency tuning curves, fourier analysis of PSTHs was carried out and the first harmonic response amplitude was calculated per spatial frequency condition.

To quantify the spatial antagonism in the receptive field of retina and LGN cells, we used the band-pass index (BPI) definition by Lee et al.,[89] which is the ratio of the spatial frequency response at the lowest frequency (R_0) to the response at the peak frequency (R_{max}):

$$BPI = R_0/R_{max} \tag{12}$$

The BPI lies between 0 and 1. BPI = 1 (low-pass spatial frequency response) indicates the receptive

field is solely driven by the center mechanism, and BPI = 0 (completely bandpass spatial frequency response) means complete surround suppression of the centers response at low spatial frequencies.

To classify cortical cells, we calculated the color-sensitivity index according to the definition by Johnson et al.:[10]

$$SI = \frac{response_{max(equiluminance)}}{response_{max(luminance)}} \quad (13)$$

where $response_{max(equiluminance)}$ is the peak response to the equiluminant grating and $response_{max(luminance)}$ is the peak response to the luminance grating.

2.8. *Implementation*

The network model was simulated using NEST 2.12.0[37] via its Python interface (PyNEST[90]). Neuron models of retinal cells were developed as extension modules linked into NEST. Van Hateren's model of primate, implemented in Python, was created following the exact description given in the publication.[69] Simulations of different trials were parallelized in the Stallo supercomputer cluster[91] based on the MPI interface. A MPI distributed-memory parallelization was implemented using the Python library *mpi4py*.[92] By running 64 processes in parallel, computation of all trials for one of the different stimulus conditions (e.g., spatial frequency) took on average about 30 minutes.

3. Results

3.1. *Achromatic light flashes*

Stimulation with light flashes is a common methodology for describing the basic properties of the cell's receptive field. A full-field spot covering the whole receptive field of retina cells elicits the well-known center-surround antagonistic response as shown in Fig. 3 A, in which both bipolar and ganglion cells functionally behave as local edge detectors overshooting the edges of the white spot.[93] Within the first 50-ms time window after stimulus onset (500-550 ms), bipolar-cell responses (L-ON and L-OFF midget bipolar cells) are predominantly driven by the center response (excitatory for L-ON bipolar cell and inhibitory for L-OFF bipolar cells) and the resulting spatial profile of cells' responses is uniform along the whole spot surface. Surround suppression of the center response clearly emerges for the second time window after stimulus onset (550-600 ms), when the response of H1 horizontal cells reaches its peak. During this time window, the response of L-ON bipolar cells located within the center of the spot is weakened because they receive strong inhibition from a great number of surrounding horizontal cells. L-ON bipolar cells situated on the spot edge, though, receive strong inhibition only from a reduced number of horizontal cells and the contribution of the excitatory center overcomes the weak inhibitory surround. A similar behavior is seen for L-OFF bipolar cells but responses have the opposite sign. The center-surround response is enhanced for ganglion cells due to the nonlinearity introduced by the sigmoid function of the synapse between bipolar and ganglion cells.

Temporal dynamics of neurons' responses to different types of light flashes are shown in Fig. 3 B: full-field black and white spots, a small white spot and a white annulus. The response properties of all cell types in the model were calibrated on the basis of similar experimental results. Thus, for stimulus types somehow correlated with light flashes, the amplitude of response in model horizontal cells and bipolar cells was adjusted to be in accordance with experimental observations of Dacey et al.[58,94] The magnitude of the firing rate of retinal ganglion cells and LGN neurons is based on data from the studies by Lee et al.[89,95] In addition, synaptic weights of LGN cells were tuned to transmit only about half of the retinal inputs they receive.[79]

In general terms, the full-field white spot evokes strong depolarizations in ON cells during the stimulus onset, followed by a rebound inhibition for the stimulus offset. The dark spot evokes responses of the opposite sign, i.e., pronounced hyperpolarization followed by rebound excitation.

While the full-field stimuli are used to show center-surround interactions as described above, the small spot (covering the receptive-field center) and the annulus allows an approximate isolation of the center and the surround responses respectively.[96] The responses of cells in the vertical pathway (retinal bipolar and ganglion cells and LGN relay cells) are greater for the center spot, in which the surround response is silenced, than for the full-field spot, which also includes surround suppression. The effects of

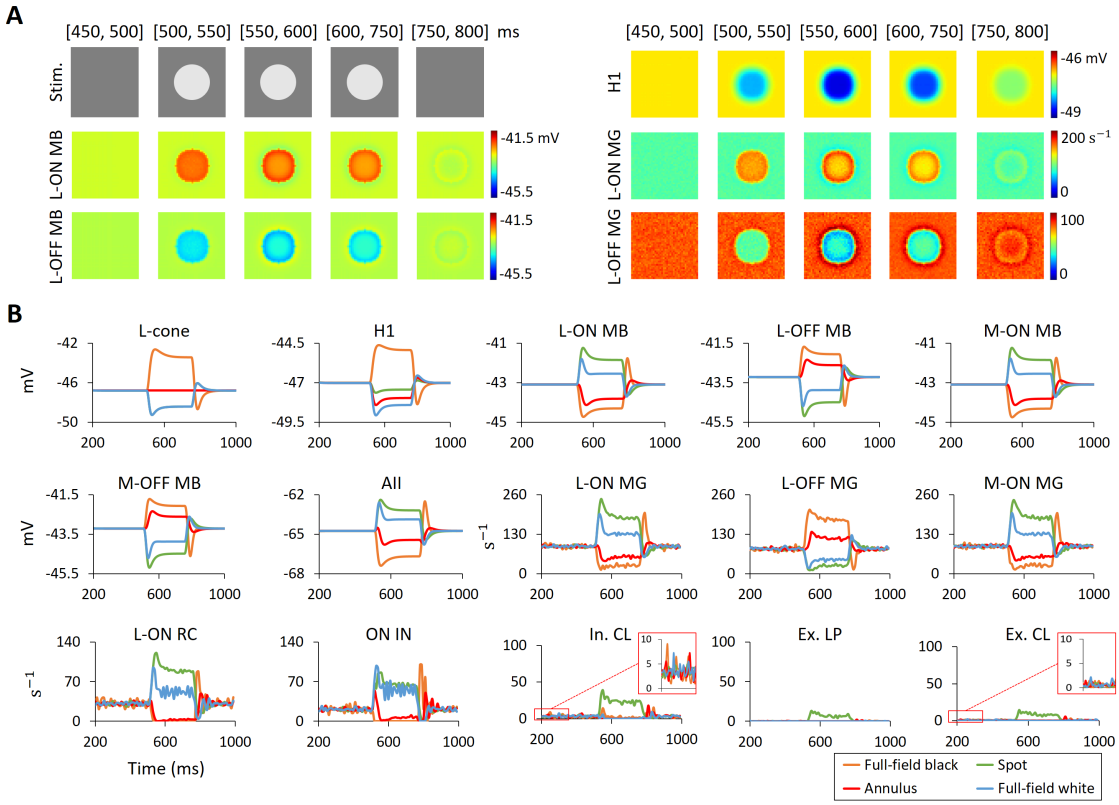

Figure 3. Model responses to different types of flashing stimuli. A: Time-averaged topographic representation of cells' responses to a full-field white spot. Activity of cells was averaged across the five time windows shown at the top of each plot. B: Trial-averaged individual responses of neurons situated in the center of each grid to a full-field black spot, a full-field white spot, a small white spot and a white annulus. Responses are either in mV (membrane potential) or s^{-1} (PSTH), where H1 is H1 horizontal cell, MB is midget bipolar cell, AII is AII amacrine cell, MG is midget ganglion cell, RC is relay-cell, IN is LGN interneuron, CL is color-luminance cortical cell and LP is luminance-preferring cortical cell.

surround suppression elicited by the full-field spot are clearly seen when the response reaches a steady state after 600 ms: e.g., the response of the L-ON midget ganglion cell is reduced to 74 % of the peak response with the center spot and to 63 % with the full-field spot. A marked increase of surround suppression is seen for relay cells (the response is reduced to 52 % with the full-field spot) as a result of the additional inhibition received through interneurons, as observed in the mammalian thalamocortical system.[97,98] Another key aspect of the comparison between responses to these two stimuli is the time-to-peak value. The full-field spot response of the ON cells shows a peak about 35 ms after stimulus onset, while the response to the center spot is shifted to 40 ms, which is within the range of values found in experiments with parvocellular cells.[72] By contrast, the peak of the surround response, activated by the annulus stimulus, is delayed by approximately 10-15 ms with respect to the center response, in agreement with experimental findings.[72]

We selected a group of cortical cells in Fig. 3 B as an example that reflects the general trend of the cortical-cell response to this type of stimuli. As expected, cortical cells respond poorly to spots and full-field stimuli.[82] Among all these stimuli, the center spot is the only one that can elicit a noticeable response, although the magnitude of the response is far from the peak firing rate of cortical cells. The model emulates two key properties of V1:[28,35] inhibitory-cell firing rates two to three times those of excitatory-cell firing rates and a low and irregular background firing between 1 and 10 s^{-1} (e.g., the background firing of excitatory cells shown in the insets of Fig. 3

B is 1-2 s^{-1}).

3.2. *Drifting sinusoidal gratings*

Cortical cells respond preferentially to an edge-like stimulus aligned along their orientation axis,[82] as exemplified by responses to drifting gratings of the cortical cells shown in Fig. 4. In the primate visual cortex, cells can reach peak firing rates of 80-100 s^{-1} when driven by their preferred gratings.[7,99] However, the response of most cells in V1 to the orientation orthogonal to the preferred orientation is often close to zero. In the study of Johnson et al.,[7] luminance-preferring cells were the most orientation selective, but there was a great deal of overlap in the distribution of orientation-selectivity ratios for the luminance-preferring and color-luminance cells. Our choice was to configure both color-luminance and luminance-preferring cells with a high orientation selectivity. As depicted in Fig. 4, the vertical grating entirely suppresses the response of the horizontally-oriented color-luminance cell.

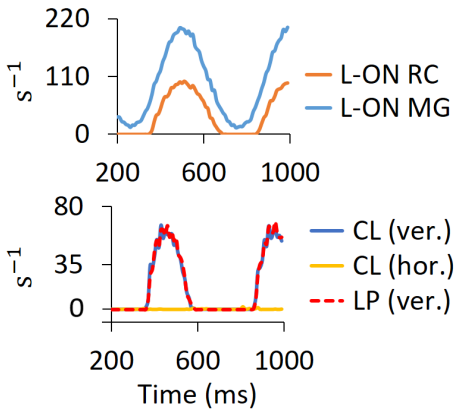

Figure 4. Model responses to a luminance grating with vertical orientation. The neurons shown are a ganglion cell (MG), a relay cell (RC), a couple of horizontally- and vertically-oriented color-luminance cells (CL) and a luminance-preferring cell (LP). The spatial frequency of the grating is 3 cpd and the temporal frequency of the drift is 2 Hz.

Spatial frequency tuning curves have been widely used to understand the neuronal basis of color mechanisms.[7,10,89,100] It is well-known that parvocellular cells multiplex luminance information (at high spatial frequencies) and chromatic information (at low spatial frequencies),[72] which means, as shown in simulation results of Fig. 5, that the response of ganglion cells and relay cells to chromatic gratings is low-pass in shape but the response to luminance gratings is band-pass. As observed for parvocellular cells near the fovea,[89,101] the luminance response of model cells shows a peak at about 3 cpd. Their responses to L- and M-cone-isolating gratings are also consistent with the responses measured experimentally to cone-isolating gratings: almost low-pass in shape but with a 180-degree phase difference at low spatial frequencies (not shown here), indicating opponency.

Table 5. Bandpass indices (BPI) of ganglion cells and relay cells in response to luminance and cone-isolating gratings.

	Luminance	Cone-isolating
Retina	0.63	0.90
LGN	0.59	0.91

However, the responses to L- and M-cone-isolating gratings show some degree of bandpass shape, as a consequence of the mixed input of L and M cones we chose for the H1 horizontal cell, prioritizing morphological studies of the primate retina. To quantify the shape of the spatial frequency tuning curves, we used the bandpass index (BPI) (see Methods, Section 2.7). According to experimental results,[89] the average BPI for midget and parvocellular cells in response to luminance gratings was near 0.4 - 0.5 and the BPI in response to cone-isolating gratings was 0.94 (although 78 % of parvocellular cells had a BPI > 0.95). The BPI calculated for the model ganglion cells is 0.63 and for the model LGN relay cells is 0.59 in response to luminance gratings (Table 5). When using a grating that isolates the receptive field center cone class, the BPI of our model cells is about 0.9. These values differ slightly from experimental values. Our model cannot reach a BPI of 0.95 in response to cone-isolating gratings because the surround circuitry is based on random cone input. However, the BPI of the model is very close to this value because the center-surround antagonism is moderate and the weight of the center response is sufficiently large compared to the weight of the surround response. On the other hand, a moderate center-surround antagonism also increases the BPI

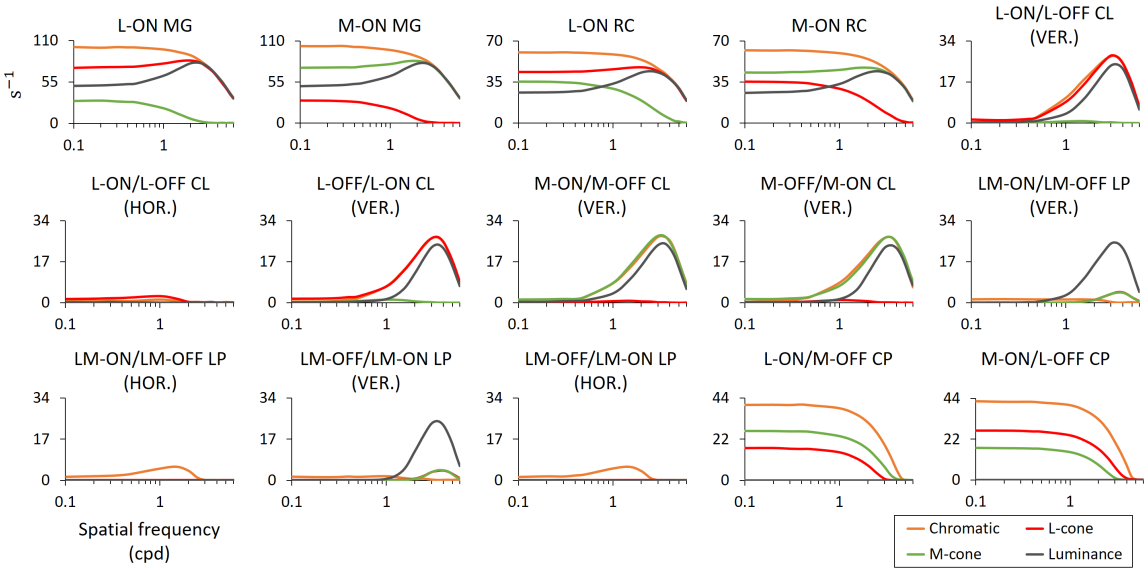

Figure 5. Spatial frequency tuning curves of neurons situated in the center of each grid using four different kinds of grating patterns: luminance, chromatic equiluminant red/green, and M- or L-cone-isolating gratings. MG is midget ganglion cell, RC is relay cell, CL is color-luminance cell, LP is luminance-preferring cell and CP is color-preferring cell. All cortical cells are excitatory cells.

for luminance gratings. It is worth mentioning that, for luminance gratings, there was much variability of BPI in the experiment and a great number of cells showed a BPI > 0.6.[89]

Spatial frequency tuning curves of cortical cells in Fig. 5 are in conformity with the responses described by Johnson et al.[7,10] Luminance-preferring cells show little or no response to chromatic gratings, but respond well to luminance gratings. The response to the luminance grating is band-pass in shape, with a peak at 3-4 cpd that is not significantly different from the range of values reported[10] for luminance-preferring cells (2-3 cpd). Color-luminance cells give comparable responses to both luminance and chromatic gratings. The preferred spatial frequency of these cells is also in the range 3-4 cpd. Color-preferring cells give large responses to chromatic gratings (low-pass in shape) and no response to luminance gratings. A qualitative evaluation of the degree of similarity between simulated and experimental responses can be made by visual comparison with Fig. 1 in the referenced paper.[10] Quantitatively, we calculated the sensitivity index (SI) of the three groups of cortical cells (see Section 2). Luminance-preferring cells have a very low sensitivity index (SI = 0.05). Color-luminance cells have a sensitivity index of about one (SI = 1.1). Color-preferring cells yield a very large sensitivity index (SI > 100). These values are in rough agreement with the range of sensitivity ratios measured.[10]

In a later study,[7] Johnson et al. complemented these results providing tuning curves to cone-isolating gratings. For color-preferring cells, the low-pass tuning curves to L- and M-cone isolating gratings, which are similar in shape and magnitude, are consistent with the tuning curves shown in Fig. 3 of the paper.[7] In our model, color-luminance cells give a large response to one cone-isolating grating and respond very weakly to the other. Experimental data also show that one of the cone-isolating gratings produces a more pronounced response.[7] However, the response to the other grating is significantly larger than zero (see simple-cell tuning curves in Fig. 2 of the publication[7]). The weaker response is produced by the grating that stimulates the receptive-field surround of the LGN cells that connect with the cortical cell. Due to the network design, these receptive-field surrounds greatly overlap and thus their responses to cone-isolating gratings roughly cancel each other out. It is interesting to note that Johnson's study was based on the entire population of V1. It is likely that neurons' responses in other layers are different

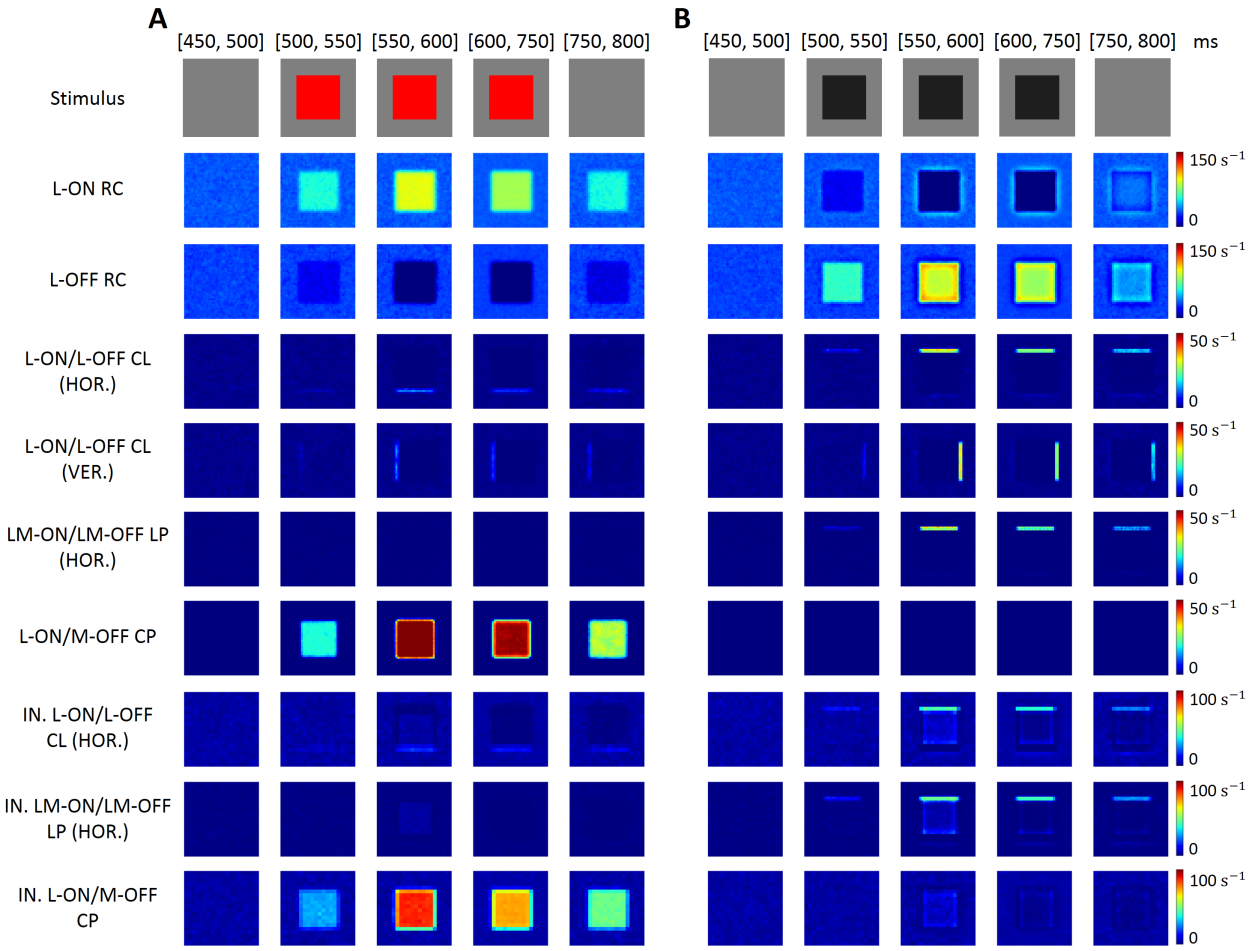

Figure 6. Time-averaged topographic representations of neurons' firing rates to spatially uniform red (A) and black (B) squares. Firing rates were averaged across the five time windows shown at the top of each plot. CL is color-luminance cell, LP is luminance-preferring cell and CP is color-preferring cell.

from responses in layer 4Cβ.

3.3. *Spatially uniform squares*

To investigate the response of model cortical cells in layer 4Cβ to color surfaces, we replicated the conditions of the experiment conducted by Zweig et al.[102] in V1. On each trial of the simulation, red and black squares (1 deg $\times$ 1 deg) were presented for 250 ms on a full-field equiluminant background (50 cd/m^2). The red square was equal in luminance to the background and the luminance contrast of the black square (80 % contrast) was adjusted to be similar to the L-M cone contrast of the red square (see Section 2.7).

Time-averaged two-dimensional representations of neural responses are shown in Fig. 6 for LGN relay cells and for different subpopulations of cortical cells. For LGN cells, L-ON relay cells are activated by the red square and L-OFF relay cells by the black square. The spatial profile of relay cells' responses is uniform along the interior of the square surface. The receptive-field surround of LGN relay cells (a mixture of L- and M-cone inputs) approximately produces a signal that is the luminance signal. We set the red square equal in luminance to the background so that the level of surround suppression in the relay-cell receptive field is the same both inside and at the edge of the red square. Thus, the effect of edge-enhancement is not seen for the red square, only for the black square.

The response of cortical color-luminance cells is consistent with their description as double-opponent cells.[20] They are oriented cells, selective for edge po-

larity and respond well to the edges of both types of squares. Luminance-preferring cells have similar properties except that they respond only to the edges of the black square. The response of color-preferring cells to the red square resembles that of LGN cells, although, unlike LGN cells, color-preferring cells are silenced in response to the black square. Populations of inhibitory cells give parallel patterns of activity but their responses are greater (see scale bars).

According to the experimental results of Zweig et al.,[102] response to the black square early after stimulus onset were edge-enhanced, in agreement with the simulation results presented here for the edge-responsive cells. These experiments show that the edges of the black square were activated 60-100 ms after stimulus onset. In the same way, the response of cortical cells in our model reaches its peak within the interval 550-600 ms (50-100 ms after stimulus onset).

4. Conclusions

In the present paper we have developed a mechanistic network model of the first stages in the primate parvocellular pathway (retina, lateral geniculate nucleus and layer 4Cβ in V1) based on two-dimensional layers of conductance-based point neurons. The main focus of this work has been on the design of the network architecture and selection of model parameter values in strict accordance with available physiological and anatomical data of the primate foveal and parafoveal vision. The model is intended to serve as a simulation tool that enables exploration of several hypotheses of the neural coding of color vision. Unlike other biophysical modeling studies of the mammalian thalamocortical system,[34,35] the present model provides a detailed mechanistic description of every stage of the visual system, including the retina. To facilitate independent validation and further scientific exploration, the model has been implemented using a well-established simulation tool, NEST 2.12.0,[37] and the code has been released as open source software.[38]

Dynamics of the neurons' membrane potential are described according to the basic equation of a single-compartment neuron model. This neuron model gives an appropriate tradeoff between computational complexity and biological accuracy and has been widely used in large-scale modeling focused on neural interactions at the level of population coding.[33,35,36] The synaptic input is modeled as a fluctuating conductance, rather than a current, because it has been suggested to be a more realistic model to capture the effects of synaptic changes on the integrative properties of cortical neurons, effects that are neglected in current-based models.[103] Moreover, it is known that there is a lack of a standardized model for neurons that communicate via graded potentials instead of spikes, as happens with most retinal neuron types.[62] Based on previous neural models that do not include action potentials,[63,64] synaptic interactions in the retina stage are described by an instantaneous sigmoid function. This function is typically defined as a direct function of some presynaptic activity measure, which, in our case, corresponds to the presynaptic membrane potential.

One key element of our model circuit is the construction of receptive fields of cortical cells, which is based on the physiological results of Johnson et al.[7,10,60] The population of cortical cells was divided into three groups: luminance-preferring (60 % of the total population), color-luminance (30 %) and color-preferring cells (10 %). Luminance-preferring and color-luminance cells have oriented receptive fields with odd-symmetry: receptive fields formed by two adjacent elongated subregions, ON and OFF, of similar weights[20,60] (see Fig. 2). Receptive fields of color-luminance cells have subregions that are fed only by a single type of relay cell so that their response is spatially tuned for equiluminant and also for luminance patterns. Receptive fields of luminance-preferring cells have subregions that receive input from two types of relay cells but always of the same sign. Luminance-preferring cells respond preferentially to achromatic patterns. Color-preferring cells are not orientation selective and have subregions that are approximately circular in shape and concentric, receiving input from both L-ON and M-OFF relay cells or from both M-ON and L-OFF relay cells.

The response of the model was validated against well-known visual stimuli commonly employed in electrophysiological experiments: disk- and ring-shaped light flashes, spatially uniform squares and sine-wave gratings of varying spatial frequency. All stimuli were configured based strictly on descriptions provided in the referenced publications and some common values (e.g., the intensity of the equiluminant background). We have shown in Section 3 that the model response captures the most important physiological properties of parvocellular cells,

e.g., ganglion cells multiplex luminance information at high spatial frequencies and chromatic information at low spatial frequencies. The spatial responses of cortical cells are also in agreement with their classification into chromatically single-opponent and double-opponent groups, and non-opponent cells selective for luminance patterns.

Consistent with our network model, De Valois and De Valois[16] proposed a multi-stage color model where chromatic and much of the achromatic information involved in vision are multiplexed in the parvocellular pathway. In the second stage of their model, the spectrally opponent retinal cells have receptive fields that respond to spatially patterned luminance increments but not to diffuse illumination. Conversely, these cells show an uniformly excitatory receptive field for an equiluminant color change. They also found that it makes little difference to the total output of the second stage of the model whether the surround of receptive fields is random or cone-specific, postulating that random connectivity is likely to be the rule in the brain. In accordance with our model, they finally developed the random-connectivity version for the second stage. The third stage of their system, assumed to occur in V1, combines these spectrally opponent responses to separate color and luminance signals. This stage presents similarities and differences with layer 4Cβ of our model. We developed receptive fields of color-preferring cells in agreement with the receptive fields used by De Valois and De Valois to extract the color signal, which sum parvocellular cells of opposite sign. The third stage of their model adds together the outputs of parvocellular cells of the same sign to produce a luminance signal. In a similar way, our luminance-preferring cells have receptive fields whose subregions receive inputs from relay cells of the same sign. However, receptive fields in their third stage do not have a spatial structure selective for orientation. As a consequence, the group of color-luminance cells is not represented in their model.

The present network model of the primate visual system is evidently simplified. The model lacks detailed dendritic/axonal morphologies and intracellular compartments. Single-compartment models are, though, a convenient oversimplification used in large-scale models of the thalamocortical system to describe neural interactions at the population level.[28–32,35] The model circuit of V1 only includes layer 4Cβ and neglects all intracortical connections among the different layers. However, the most significant transformations to color signals may occur at the next synapse (layers 2/3 and 5/6).[20] The present model also assumes static synapses while a number of studies have shown the existence of short-term plasticity in different synapses of the thalamocortical circuit, i.e., short-term depression at the retinogeniculate[104] and geniculocortical[105] synapses, as well as in the feedback connection from cortex to LGN.[106] Such extensions opens up for an even richer dynamical repertoire of the circuit, and would be an interesting topic for a future study using the present model as a starting point.

The existence and perceptual importance of a neuronal response to the interior of color surfaces is still under debate. An interesting topic for a future study would be to investigate the population response of the model to color surfaces. Some studies found that color surface signals of V1 tend to be much weaker and remain unaltered when the perceptual color change occurs.[107] Other researchers postulate the existence, under certain conditions, of a mechanism of *filling-in* as a process by which neural activity of edges is spread towards the center.[102] The recent findings by Zweig and coauthors[102] show that representations of chromatic and achromatic surfaces in V1 are not similar over time. While the responses to both types of surfaces were edge-enhanced throughout the stimulus presentation, only achromatic surfaces activated a late *filling-in* of the center's response. Their results support a horizontal-connection-mediated neuronal *filling-in* mechanism.

The interaction between brightness and color can cause the color appearance of an object to change when viewing the object against surrounds of different brightness. It has been demonstrated that brightness and color interact strongly already within V1 by using chromatic visual-evoked potential.[108] The main finding is that brightness-color interactions take place at the edges of the surface, where it is suggested that luminance-preferring cells produce an amount of inhibition proportional to the level of luminance contrast. An interesting next application of the present model would be to explore the response properties to color surfaces when the luminance of the surround is changed and whether the model can replicate the brightness-color interactions observed in V1.

It has been proposed that color information in the cortex is encoded in the distribution of activity across the population of neurons[20] and recent studies have focused on measuring population activity patterns to chromatic and achromatic stimuli.[102,109] The present simulation platform brings a great opportunity for investigation of neuronal interactions of color processing at the population level. Further exploration of the possibilities for population coding may lead to a new understanding of color perception.

Acknowledgments

This work was supported by MINECO-FEDER TIN2016-81041-R grant and the research project P11-TIC-7983 of Junta of Andalucia (Spain), co-financed by the European Regional Development Fund (ERDF). P. Martínez-Cañada was supported by the PhD scholarship FPU13/01487, awarded by the Government of Spain, FPU program.

Bibliography

1. K. R. Gegenfurtner, Cortical mechanisms of colour vision, *Nature reviews. Neuroscience* **4**(7) (2003) p. 563.
2. I. Spence, P. Wong, M. Rusan and N. Rastegar, How color enhances visual memory for natural scenes, *Psychological Science* **17**(1) (2006) 1–6.
3. K. R. Gegenfurtner and J. Rieger, Sensory and cognitive contributions of color to the recognition of natural scenes, *Current Biology* **10**(13) (2000) 805–808.
4. P. Gouras, Identification of cone mechanisms in monkey ganglion cells, *The Journal of physiology* **199**(3) (1968) 533–547.
5. R. L. De Valois, I. Abramov and G. H. Jacobs, Analysis of response patterns of lgn cells, *JOSA* **56**(7) (1966) 966–977.
6. G. D. Horwitz and C. A. Hass, Nonlinear analysis of macaque v1 color tuning reveals cardinal directions for cortical color processing, *Nature neuroscience* **15**(6) (2012) 913–919.
7. E. N. Johnson, M. J. Hawken and R. Shapley, The orientation selectivity of color-responsive neurons in macaque v1, *Journal of Neuroscience* **28**(32) (2008) 8096–8106.
8. B. R. Conway and M. S. Livingstone, Spatial and temporal properties of cone signals in alert macaque primary visual cortex, *Journal of Neuroscience* **26**(42) (2006) 10826–10846.
9. R. C. Reid and R. M. Shapley, Space and time maps of cone photoreceptor signals in macaque lateral geniculate nucleus, *Journal of Neuroscience* **22**(14) (2002) 6158–6175.
10. E. N. Johnson, M. J. Hawken and R. Shapley, The spatial transformation of color in the primary visual cortex of the macaque monkey, *Nature neuroscience* **4**(4) (2001) p. 409.
11. A. M. Derrington, J. Krauskopf and P. Lennie, Chromatic mechanisms in lateral geniculate nucleus of macaque., *The Journal of physiology* **357**(1) (1984) 241–265.
12. E. N. Johnson and K. T. Mullen, Color in the cortex (2016) 189–217.
13. M. S. Livingstone and D. H. Hubel, Psychophysical evidence for separate channels for the perception of form, color, movement, and depth, *Journal of Neuroscience* **7**(11) (1987) 3416–3468.
14. J. Krauskopf, D. R. Williams and D. W. Heeley, Cardinal directions of color space, *Vision research* **22**(9) (1982) 1123–1131.
15. J. Hérault, A model of colour processing in the retina of vertebrates: From photoreceptors to colour opposition and colour constancy phenomena, *Neurocomputing* **12**(2) (1996) 113–129.
16. R. L. De Valois and K. K. De Valois, A multi-stage color model, *Vision research* **33**(8) (1993) 1053–1065.
17. D. M. Dacey, Parallel pathways for spectral coding in primate retina, *Annual review of neuroscience* **23**(1) (2000) 743–775.
18. D. M. Dacey, Primate retina: cell types, circuits and color opponency, *Progress in retinal and eye research* **18**(6) (1999) 737–763.
19. B. B. Boycott, J. E. Dowling and H. Kolb, Organization of the primate retina: light microscopy, *Philosophical Transactions of the Royal Society of London. Series B, Biological Sciences* (1969) 109–184.
20. R. Shapley and M. J. Hawken, Color in the cortex: single-and double-opponent cells, *Vision research* **51**(7) (2011) 701–717.
21. S. G. Solomon and P. Lennie, The machinery of colour vision, *Nature reviews. Neuroscience* **8**(4) (2007) p. 276.
22. L. C. Sincich and J. C. Horton, The circuitry of v1 and v2: integration of color, form, and motion, *Annu. Rev. Neurosci.* **28** (2005) 303–326.
23. V. Perry, R. Oehler and A. Cowey, Retinal ganglion cells that project to the dorsal lateral geniculate nucleus in the macaque monkey, *Neuroscience* **12**(4) (1984) 1101–1123.
24. P. Martínez-Cañada, C. Morillas and F. Pelayo, A conductance-based neuronal network model for color coding in the primate foveal retina, *Natural and Artificial Computation for Biomedicine and Neuroscience: International Work-Conference on the Interplay Between Natural and Artificial Computation, IWINAC 2017, La Coruña, Spain, June 19-23, 2017* (2017) 63–74.

25. H. Momiji, M. W. Hankins, A. A. Bharath and C. Kennard, A numerical study of red-green colour opponent properties in the primate retina, *European Journal of Neuroscience* **25**(4) (2007) 1155–1165.
26. H. Momiji, A. A. Bharath, M. W. Hankins and C. Kennard, Numerical study of short-term afterimages and associate properties in foveal vision, *Vision research* **46**(3) (2006) 365–381.
27. V. A. Billock, Cortical simple cells can extract achromatic information from the multiplexed chromatic and achromatic signals in the parvocellular pathway, *Vision research* **35**(16) (1995) 2359–2369.
28. L. Chariker, R. Shapley and L.-S. Young, Orientation selectivity from very sparse lgn inputs in a comprehensive model of macaque v1 cortex, *Journal of Neuroscience* **36**(49) (2016) 12368–12384.
29. W. Zhu, D. Xing, M. Shelley and R. Shapley, Correlation between spatial frequency and orientation selectivity in v1 cortex: implications of a network model, *Vision research* **50**(22) (2010) 2261–2273.
30. L. Tao, M. Shelley, D. McLaughlin and R. Shapley, An egalitarian network model for the emergence of simple and complex cells in visual cortex, *Proceedings of the National Academy of Sciences* **101**(1) (2004) 366–371.
31. D. McLaughlin, R. Shapley and M. Shelley, Large-scale modeling of the primary visual cortex: influence of cortical architecture upon neuronal response, *Journal of Physiology-Paris* **97**(2) (2003) 237–252.
32. D. McLaughlin, R. Shapley, M. Shelley and D. J. Wielaard, A neuronal network model of macaque primary visual cortex (v1): Orientation selectivity and dynamics in the input layer 4cα, *Proceedings of the National Academy of Sciences* **97**(14) (2000) 8087–8092.
33. M. H. Hennig and F. Wörgötter, Effects of fixational eye movements on retinal ganglion cell responses: A modelling study, *Frontiers in computational neuroscience* **1** (2007).
34. E. M. Izhikevich and G. M. Edelman, Large-scale model of mammalian thalamocortical systems, *Proceedings of the national academy of sciences* **105**(9) (2008) 3593–3598.
35. S. Hill and G. Tononi, Modeling sleep and wakefulness in the thalamocortical system, *Journal of neurophysiology* **93**(3) (2005) 1671–1698.
36. A. Destexhe, D. Contreras and M. Steriade, Mechanisms underlying the synchronizing action of corticothalamic feedback through inhibition of thalamic relay cells, *Journal of neurophysiology* **79**(2) (1998) 999–1016.
37. S. Kunkel, A. Morrison, P. Weidel, J. M. Eppler, A. Sinha, W. Schenck, M. Schmidt, S. B. Vennemo, J. Jordan, A. Peyser, D. Plotnikov, S. Graber, T. Fardet, D. Terhorst, H. Mrk, G. Trensch, A. Seeholzer, R. Deepu, J. Hahne, I. Blundell, T. Ippen, J. Schuecker, H. Bos, S. Diaz, E. Hagen, S. Mahmoudian, C. Bachmann, M. E. Lepperd, O. Breitwieser, B. Golosio, H. Rothe, H. Setareh, M. Djurfeldt, T. Schumann, A. Shusharin, J. Garrido, E. B. Muller, A. Rao, J. H. Vieites and H. E. Plesser, Nest 2.12.0 (March 2017).
38. P. Martínez-Cañada, Github code repository: https://github.com/pablomc88.
39. T. A. Chaplin, H.-H. Yu and M. G. Rosa, Representation of the visual field in the primary visual area of the marmoset monkey: Magnification factors, point-image size, and proportionality to retinal ganglion cell density, *Journal of Comparative Neurology* **521**(5) (2013) 1001–1019.
40. B. Dow, A. Snyder, R. Vautin and R. Bauer, Magnification factor and receptive field size in foveal striate cortex of the monkey, *Experimental brain research* **44**(2) (1981) 213–228.
41. D. M. Dacey and M. R. Petersen, Dendritic field size and morphology of midget and parasol ganglion cells of the human retina., *Proceedings of the National Academy of sciences* **89**(20) (1992) 9666–9670.
42. R. H. Masland, The fundamental plan of the retina, *Nature neuroscience* **4**(9) (2001) 877–886.
43. J. B. Demb and J. H. Singer, Intrinsic properties and functional circuitry of the aii amacrine cell, *Visual neuroscience* **29**(1) (2012) 51–60.
44. M. B. Manookin, D. L. Beaudoin, Z. R. Ernst, L. J. Flagel and J. B. Demb, Disinhibition combines with excitation to extend the operating range of the off visual pathway in daylight, *Journal of Neuroscience* **28**(16) (2008) 4136–4150.
45. J. Snellman, T. Kaur, Y. Shen and S. Nawy, Regulation of on bipolar cell activity, *Progress in retinal and eye research* **27**(4) (2008) 450–463.
46. S. Nawy and C. E. Jahr, Suppression by glutamate of cgmp-activated conductance in retinal bipolar cells, *Nature* **346**(6281) (1990) 269–271.
47. J. A. Hirsch, X. Wang, F. T. Sommer and L. M. Martinez, How inhibitory circuits in the thalamus serve vision, *Annual review of neuroscience* **38** (2015) 309–329.
48. J. R. Wilson, Synaptic organization of individual neurons in the macaque lateral geniculate nucleus, *Journal of Neuroscience* **9**(8) (1989) 2931–2953.
49. C. R. Michael, Retinal afferent arborization patterns, dendritic field orientations, and the segregation of function in the lateral geniculate nucleus of the monkey, *Proceedings of the National Academy of Sciences* **85**(13) (1988) 4914–4918.
50. P. H. Schiller, The connections of the retinal on and off pathways to the lateral geniculate nucleus of the monkey, *Vision Research* **24**(9) (1984) 923–932.
51. J. R. Wilson, D. M. Forestner and R. P. Cramer, Quantitative analyses of synaptic contacts of interneurons in the dorsal lateral geniculate nucleus of the squirrel monkey, *Visual neuroscience* **13**(6)

(1996) 1129–1142.
52. V. A. Casagrande, D. W. Royal and G. Sáry, Geniculate nucleus (lgn), *The primate visual system: a comparative approach* (2005) p. 191.
53. C. Beaulieu, Z. Kisvarday, P. Somogyi, M. Cynader and A. Cowey, Quantitative distribution of gaba-immunopositive and-immunonegative neurons and synapses in the monkey striate cortex (area 17), *Cerebral Cortex* **2**(4) (1992) 295–309.
54. A. Wohrer and P. Kornprobst, Virtual retina: a biological retina model and simulator, with contrast gain control, *Journal of computational neuroscience* **26**(2) (2009) 219–249.
55. G. T. Einevoll and P. Heggelund, Mathematical models for the spatial receptive-field organization of nonlagged x-cells in dorsal lateral geniculate nucleus of cat, *Visual Neuroscience* **17**(6) (2000) 871–885.
56. H. E. Plesser and K. Austvoll, Specification and generation of structured neuronal network models with the nest topology module, *BMC Neuroscience* **10**(1) (2009) p. P56.
57. S. Song, P. J. Sjöström, M. Reigl, S. Nelson and D. B. Chklovskii, Highly nonrandom features of synaptic connectivity in local cortical circuits, *PLoS biology* **3**(3) (2005) p. e68.
58. D. Dacey, O. S. Packer, L. Diller, D. Brainard, B. Peterson and B. Lee, Center surround receptive field structure of cone bipolar cells in primate retina, *Vision research* **40**(14) (2000) 1801–1811.
59. D. C. Van Essen, W. T. Newsome and J. H. Maunsell, The visual field representation in striate cortex of the macaque monkey: asymmetries, anisotropies, and individual variability, *Vision research* **24**(5) (1984) 429–448.
60. E. N. Johnson, M. J. Hawken and R. Shapley, Cone inputs in macaque primary visual cortex, *Journal of Neurophysiology* **91**(6) (2004) 2501–2514.
61. P. Martínez-Cañada, C. Morillas, B. Pino, E. Ros and F. Pelayo, A computational framework for realistic retina modeling, *International Journal of Neural Systems* **26**(07) (2016) p. 1650030.
62. M. H. Hennig, K. Funke and F. Wörgötter, The influence of different retinal subcircuits on the nonlinearity of ganglion cell behavior, *Journal of Neuroscience* **22**(19) (2002) 8726–8738.
63. R. G. Smith, Simulation of an anatomically defined local circuit: the cone-horizontal cell network in cat retina, *Visual neuroscience* **12**(03) (1995) 545–561.
64. A. Destexhe, Z. F. Mainen, T. J. Sejnowski *et al.*, Synaptic currents, neuromodulation, and kinetic models, *The handbook of brain theory and neural networks* **66** (1995) 617–648.
65. M. Steriade, I. Timofeev and F. Grenier, Natural waking and sleep states: a view from inside neocortical neurons, *Journal of neurophysiology* **85**(5) (2001) 1969–1985.
66. A. C. Arman and A. P. Sampath, Dark-adapted response threshold of off ganglion cells is not set by off bipolar cells in the mouse retina, *Journal of neurophysiology* **107**(10) (2012) 2649–2659.
67. D. Ulrich and J. R. Huguenard, Nucleus-specific chloride homeostasis in rat thalamus, *Journal of Neuroscience* **17**(7) (1997) 2348–2354.
68. A. Casti, F. Hayot, Y. Xiao and E. Kaplan, A simple model of retina-lgn transmission, *Journal of computational neuroscience* **24**(2) (2008) 235–252.
69. H. van Hateren, A cellular and molecular model of response kinetics and adaptation in primate cones and horizontal cells, *Journal of vision* **5**(4) (2005) 5–5.
70. N. Vardi, L.-L. Zhang, J. A. Payne and P. Sterling, Evidence that different cation chloride cotransporters in retinal neurons allow opposite responses to gaba, *Journal of Neuroscience* **20**(20) (2000) 7657–7663.
71. L. J. Croner and E. Kaplan, Receptive fields of p and m ganglion cells across the primate retina, *Vision research* **35**(1) (1995) 7–24.
72. E. Kaplan and E. Benardete, The dynamics of primate retinal ganglion cells, *Progress in brain research* **134** (2001) 17–34.
73. H. Barlow and W. Levick, Changes in the maintained discharge with adaptation level in the cat retina, *The Journal of Physiology* **202**(3) (1969) 699–718.
74. L. M. Martinez, M. Molano-Mazón, X. Wang, F. T. Sommer and J. A. Hirsch, Statistical wiring of thalamic receptive fields optimizes spatial sampling of the retinal image, *Neuron* **81**(4) (2014) 943–956.
75. E. Sánchez, R. Ferreiroa, A. Arias and L. M. Martínez, Image sharpness and contrast tuning in the early visual pathway, *International Journal of Neural Systems* **27**(08) (2017) p. 1750045.
76. P. Arcelli, C. Frassoni, M. Regondi, S. De Biasi and R. Spreafico, Gabaergic neurons in mammalian thalamus: a marker of thalamic complexity?, *Brain research bulletin* **42**(1) (1997) 27–37.
77. B. Babadi, A. Casti, Y. Xiao, E. Kaplan and L. Paninski, A generalized linear model of the impact of direct and indirect inputs to the lateral geniculate nucleus, *Journal of Vision* **10**(10) (2010) 22–22.
78. C. Hunt, D. Pang and E. Jones, Distribution and density of gaba cells in intralaminar and adjacent nuclei of monkey thalamus, *Neuroscience* **43**(1) (1991) 185–196.
79. H. J. Alitto and W. M. Usrey, Dynamic properties of thalamic neurons for vision, *Progress in brain research* **149** (2005) 83–90.
80. J. S. Lund, A. Angelucci and P. C. Bressloff, Anatomical substrates for functional columns in macaque monkey primary visual cortex, *Cerebral Cortex* **13**(1) (2003) 15–24.
81. D. Latawiec, K. A. Martin and V. Meskenaite, Termination of the geniculocortical projection in

the striate cortex of macaque monkey: a quantitative immunoelectron microscopic study, *Journal of Comparative Neurology* **419**(3) (2000) 306–319.
82. M. J. Hawken and A. J. Parker, Spatial properties of neurons in the monkey striate cortex, *Proceedings of the Royal Society of London B: Biological Sciences* **231**(1263) (1987) 251–288.
83. L. C. Katz, C. D. Gilbert and T. N. Wiesel, Local circuits and ocular dominance columns in monkey striate cortex, *Journal of Neuroscience* **9**(4) (1989) 1389–1399.
84. D. Fitzpatrick, J. S. Lund and G. G. Blasdel, Intrinsic connections of macaque striate cortex: afferent and efferent connections of lamina 4c, *Journal of Neuroscience* **5**(12) (1985) 3329–3349.
85. Z. Kisvarday, A. Cowey and P. Somogyi, Synaptic relationships of a type of gaba-immunoreactive neuron (clutch cell), spiny stellate cells and lateral geniculate nucleus afferents in layer ivc of the monkey striate cortex, *Neuroscience* **19**(3) (1986) 741–761.
86. R. Shapley, M. Hawken and D. Xing, The dynamics of visual responses in the primary visual cortex, *Progress in brain research* **165** (2007) 21–32.
87. J. S. Anderson, M. Carandini and D. Ferster, Orientation tuning of input conductance, excitation, and inhibition in cat primary visual cortex, *Journal of neurophysiology* **84**(2) (2000) 909–926.
88. C. Stromeyer, G. Cole and R. Kronauer, Second-site adaptation in the red-green chromatic pathways, *Vision Research* **25**(2) (1985) 219–237.
89. B. B. Lee, R. M. Shapley, M. J. Hawken and H. Sun, Spatial distributions of cone inputs to cells of the parvocellular pathway investigated with cone-isolating gratings, *JOSA A* **29**(2) (2012) A223–A232.
90. J. M. Eppler, M. Helias, E. Muller, M. Diesmann and M.-O. Gewaltig, Pynest: a convenient interface to the nest simulator, *Frontiers in neuroinformatics* **2** (2008).
91. HPC group - UiT The Arctic University of Norway, Stallo supercomputer (2016).
92. L. D. Dalcin, R. R. Paz, P. A. Kler and A. Cosimo, Parallel distributed computing using python, *Advances in Water Resources* **34**(9) (2011) 1124–1139.
93. R. H. Masland, The neuronal organization of the retina, *Neuron* **76**(2) (2012) 266–280.
94. D. M. Dacey, B. B. Lee, D. K. Stafford, J. Pokorny and V. C. Smith, Horizontal cells of the primate retina: cone specificity without spectral opponency, *Science* **271**(5249) (1996) p. 656.
95. B. B. Lee, Color coding in the primate visual pathway: a historical view, *JOSA A* **31**(4) (2014) A103–A112.
96. E. A. Benardete and E. Kaplan, The receptive field of the primate p retinal ganglion cell, i: Linear dynamics, *Visual neuroscience* **14**(1) (1997) 169–185.
97. P. Martínez-Cañada, M. H. Mobarhan, G. Halnes, M. Fyhn, C. Morillas, F. Pelayo, G. T. Einevoll *et al.*, Biophysical network modeling of the dLGN circuit: Effects of cortical feedback on spatial response properties of relay cells, *PLoS computational biology* **14**(1) (2018) p. e1005930.
98. O. Ruksenas, I. Fjeld and P. Heggelund, Spatial summation and center-surround antagonism in the receptive field of single units in the dorsal lateral geniculate nucleus of cat: comparison with retinal input, *Visual neuroscience* **17**(6) (2000) 855–870.
99. M. Hawken, R. M. Shapley and D. Grosof, Temporal-frequency selectivity in monkey visual cortex, *Visual neuroscience* **13**(3) (1996) 477–492.
100. J. D. Crook, M. B. Manookin, O. S. Packer and D. M. Dacey, Horizontal cell feedback without cone type-selective inhibition mediates red–green color opponency in midget ganglion cells of the primate retina, *Journal of Neuroscience* **31**(5) (2011) 1762–1772.
101. P. Lennie and J. A. Movshon, Coding of color and form in the geniculostriate visual pathway (invited review), *JOSA A* **22**(10) (2005) 2013–2033.
102. S. Zweig, G. Zurawel, R. Shapley and H. Slovin, Representation of color surfaces in v1: edge enhancement and unfilled holes, *Journal of Neuroscience* **35**(35) (2015) 12103–12115.
103. M. J. Richardson and W. Gerstner, Conductance versus current-based integrate-and-fire neurons: Is there qualitatively new behaviour?, *Lausanne lecture* .
104. A. Kielland and P. Heggelund, Ampa and nmda currents show different short-term depression in the dorsal lateral geniculate nucleus of the rat, *The Journal of physiology* **542**(1) (2002) 99–106.
105. C. E. Boudreau and D. Ferster, Short-term depression in thalamocortical synapses of cat primary visual cortex, *Journal of Neuroscience* **25**(31) (2005) 7179–7190.
106. J. Turner and T. Salt, Characterization of sensory and corticothalamic excitatory inputs to rat thalamocortical neurones in vitro, *The Journal of Physiology* **510**(3) (1998) 829–843.
107. H. S. Friedman, H. Zhou and R. Heydt, The coding of uniform colour figures in monkey visual cortex, *The Journal of physiology* **548**(2) (2003) 593–613.
108. D. Xing, A. Ouni, S. Chen, H. Sahmoud, J. Gordon and R. Shapley, Brightness–color interactions in human early visual cortex, *Journal of Neuroscience* **35**(5) (2015) 2226–2232.
109. G. Zurawel, I. Ayzenshtat, S. Zweig, R. Shapley and H. Slovin, A contrast and surface code explains complex responses to black and white stimuli in v1, *Journal of Neuroscience* **34**(43) (2014) 14388–14402.